Chapter 1

Enhancing the Greenhouse Gas Conversion Efficiency in Microwave Discharges by Power Modulation

Nikolay Britun, Guoxing Chen, Tiago Silva,
Thomas Godfroid,
Marie-Paule Delplancke-Ogletree and Rony Snyders

Additional information is available at the end of the chapter

http://dx.doi.org/10.5772/67875

Abstract

Scientific interest to the plasma-assisted greenhouse gas conversion continuously increases nowadays, as a part of the global Green Energy activities. Among the plasma sources suitable for conversion of CO_2 and other greenhouse gases, the non-equilibrium (low-temperature) discharges where the electron temperature is considerably higher than the gas temperature, represent special interest. The flowing gas discharges sustained by microwave radiation are proven to be especially suitable for molecular gas conversion due to high degree of non-equilibrium they possess. In this Chapter the optimization of CO_2 conversion efficiency in microwave discharges working in pulsed regime is considered. The pulsed energy delivery represents new approach for maximization of CO_2 conversion solely based on the discharge "fine-tuning", i. e. without the additional power expenses. In our work several discharge parameters along the gas flow direction in the discharge have been studied using various diagnostic techniques, such as optical actinometry, laser-induced fluorescence, and gas chromatography. The results show that CO_2 conversion efficiency can be essentially increased solely based on the plasma pulse frequency tuning. The obtained results are explained by the relation between the plasma pulse parameters and the characteristic time of the relevant energy transfer processes in the discharge.

Keywords: green energy, greenhouse gas decomposition, plasma-assisted CO_2 conversion, power modulation, optical spectroscopy, laser spectroscopy, optical diagnostics

1. Introduction

The basic green energy activities include reduction of the greenhouse gas emission, in particular the emission of CO_2, development and implementation of the green energy sources, as well as the local conversion, reforming and utilization of the greenhouse gases (see **Figure 1**). The last activities are represented by the well-known carbon capture and storage (CCS) and carbon capture and utilization (CCU) techniques being under intensive development during the last decades [1, 2]. Among the approaches suitable for local conversion of the greenhouse gases, and in particular CO_2, the plasma-assisted conversion based on decomposition of the molecules of interest in the low-temperature discharges is of a special interest. The efficiency of such a conversion depends on various factors, such as the proper choice of plasma source, as well as its careful optimization. The plasma source optimization in this case implies tuning the fundamental physical parameters, such as the electron density and temperature, the vibrational excitation of the molecules of interest, the discharge pressure, the residence time of the molecules in the active zone, etc. For successful optimization detailed plasma source characterization is required, preferably using nonintrusive *in-situ* plasma diagnostics methods [3] often combined with plasma modeling [4].

Since the end of 1970s the utilization of low-temperature discharges is considered as a rather promising approach for molecular gas decomposition [5, 6], which can be applied for conversion of CO_2 as well as the other greenhouse gases. It is well-known that the low-temperature plasma discharges represent unique media where selectivity toward the various plasma chemical processes can be realized [6, 7]. This is a result of the high level of nonequilibrium between the main

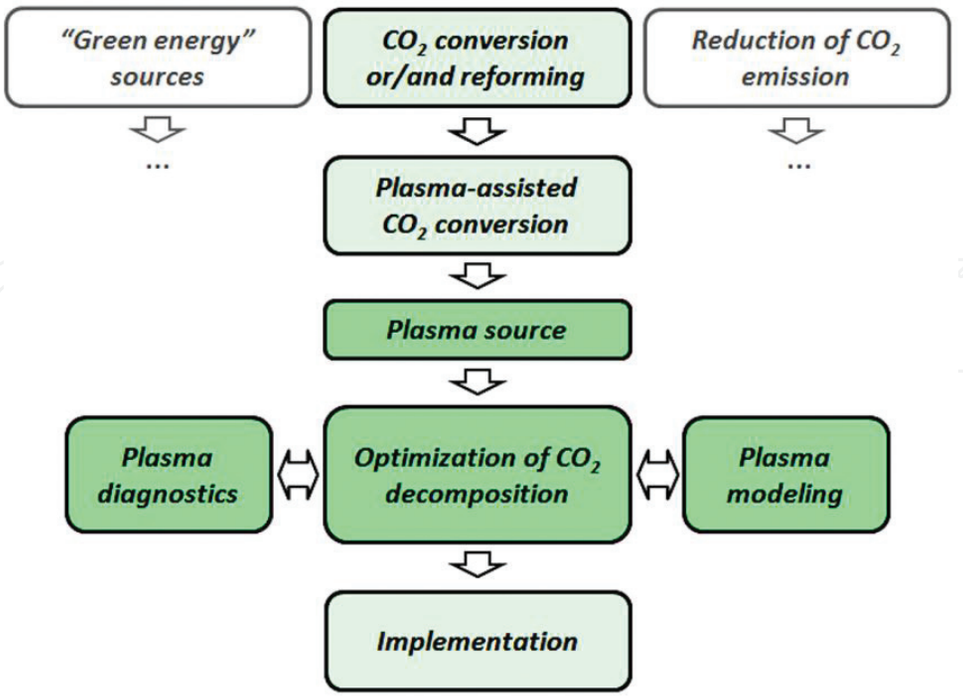

Figure 1. The role of plasma-assisted CO_2 conversion among the other green energy activities.

degrees of excitation in the discharge, such as electronic, translational, rotational, and vibrational ones. At the same time, as also shown previously, the vibrational excitation is particularly crucial for molecular dissociation in many cases [7, 8]. A high degree of nonequilibrium is especially pronounced in the microwave (MW) discharges where 90-95% of the applied electro-magnetic field energy is absorbed by plasma electrons further transmitting their energy to the vibrationally excited molecular states, while the gas temperature remains relatively low, typically about a thousand degree K or lower [6, 9].

A decisive role of the asymmetric vibrational mode of CO_2 (see below) for its efficient plasma-based decomposition has also been deduced based on the past research. The mentioned efficiency is defined, however, by several mechanisms working along with the mentioned vibrational excitation, such as: (i) fast excitation of the CO_2 asymmetric mode by plasma electrons as a result of the electron-vibrational (e-V) energy transfer, (ii) several orders of magnitude faster vibrational-vibrational (V-V) energy transfer, providing fast vibrational excitation of CO_2 molecules up to the dissociative level (≈5.5 eV), and (iii) rather slow vibrational-translational (V-T) transfer. The fast V-V process facilitates so-called vibrational "ladder climbing," i.e., fast excitation of the highly excited vibrational states of CO_2 result in its dissociation [6]. The low gas temperature in the discharge, on the other hand, is important for keeping the V-T energy transfer at a relatively low level, thus sustaining the vibrational excitation for a longer time. This time may vary from few μs to tens of ms, depending on the discharge parameters, as discussed below in this Chapter. As a result, the energy efficiency (defined below) up to 0.8 in the subsonic [10] and about 0.9 in a supersonic [11] gas flows may be achieved in the microwave plasmas. The nonequilibrium discharge conditions can also be effectively realized in the other discharges, for example in a gliding arc plasma (GAP) as a result of the arc length extension resulting in gas cooling [12].

Nowadays, the scientific interest to the greenhouse gas decomposition in the low-temperature discharges is growing. This is related to both low-pressure and high-pressure (atmospheric) cases. Apart from the general green energy trends, the growing interest is particularly based on the fast development of the scientific tools targeted to advanced nonintrusive discharge diagnostics as well as the powerful data processing systems, which are crucial for discharge kinetic modeling.

Talking in particular about the MW plasma sources we should note that along with their general effectiveness for molecular gas decomposition, the *power modulation effect* is known to be an additional alternative for enhancing the CO_2 conversion in these discharges [13]. To realize this effect, an electromagnetic wave with a filling frequency in the GHz range (serving to sustain the discharge) is periodically modulated by nearly squared pulses with a certain repetition rate, typically in the kHz range. Such modulation might be very important when the vibrational excitation is involved in a molecular decomposition process, as in the CO_2 case [6]. Since in the pulsed MW discharges the characteristic time of V-T energy transfer may be comparable to the typical plasma pulse repetition period (μs–ms range), a resonance-like effect between the power delivery and the energy transfer processes may be achieved. Thus, the periodic power delivery in these discharges represents an additional way for improving the efficiency of CO_2 conversion, at the same time requiring understanding of the corresponding physical processes. An optimization performed without increasing of the total power consumption might be extremely beneficial from the practical point of view.

In spite of the numerous works devoted to plasma-based greenhouse gas conversion in the MW discharges [11, 14, 15], dielectric barrier discharges (DBDs) [16–21], GAPs [22–24], radio-frequency (RF) discharges [25], as well as in different discharges using plasma catalysis [14, 26–28], the effects of CO_2 conversion and power modulation are still far from being understood fully. The number of the research works in this domain is also very limited, mainly by the theoretical speculations of the usability of pulsed plasma regime in MW and DBD cases [29], as well as by few experimental evidences of the pulsed discharge, benefits so far only shown for DBD case [17–19]. At the same time, the domain of the power modulation in MW low-temperature plasmas, representing one of the most promising nonequilibrium media for selective plasma chemistry, remains mainly unexplored. This chapter addresses the mentioned gap by demonstrating the importance of power modulation in the kHz range for improving the CO_2 decomposition in microwave discharges.

2. The basics of plasma-assisted CO_2 conversion

2.1. The structure and dissociation of CO_2 molecule

The structure of CO_2 molecule is schematically shown in **Figure 2**. This triatomic molecule possesses three vibrational modes, namely the symmetric stretch mode (with the main vibrational energy gap equal to about 0.17 eV), the double-degenerated bending mode (0.083 eV), and the asymmetric mode (0.291 eV). The different energy gaps for the listed modes define the differences in the energy transfer rates between them and the translational particle motion (V-T transfer), as discussed in Section 2.3. The vibrational excitation states for CO_2 are normally denoted through three vibrational quantum numbers corresponding to symmetric (v_1), bending (v_2), and asymmetric (v_3) vibrational modes.

One of the possible pathways for CO_2 decomposition is the electron impact dissociation:

$$CO_2 + e \rightarrow CO + O + e \ (\text{the energy required is } \approx 5.5 \text{ eV}). \tag{1}$$

However, as a result of recombination of atomic O with vibrationally excited CO_2 (denoted as CO_2^{vibr}) another CO molecule can be produced [6], and an effective energy per one produced CO molecule becomes ≈ 2.9 eV:

$$O + CO_2^{vibr} \rightarrow CO + O_2 (\text{the energy required is } \approx 0.3 \text{ eV}). \tag{2}$$

As mentioned earlier, the actual CO_2 dissociation strongly relies of the e-V energy transfer resulting in the excitation of the lowest vibrational states of CO_2 molecule, e.g.:

$$e + CO_2 \rightarrow CO_2(0, 0, 1) + e, \tag{3}$$

where the parenthesized numbers represent the vibrational quantum numbers mentioned above. The excitation of higher vibrational states is occurring at the same time as a result of the fast energy transfer between the different vibrational states within the same vibrational mode (i.e., V-V transfer), e.g.:

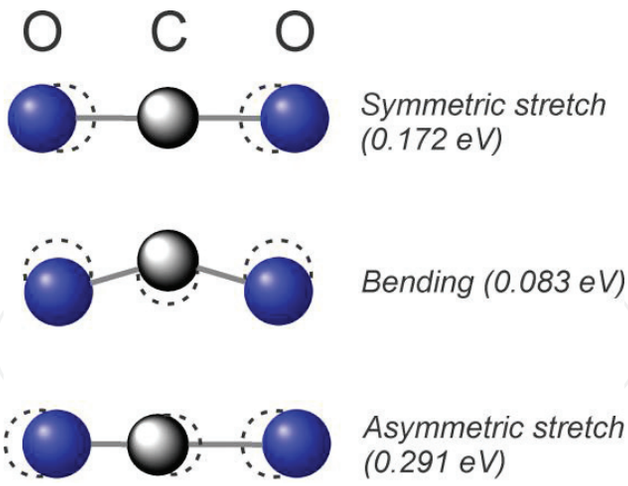

Figure 2. The structure of CO_2 molecule showing three vibrational modes. The first quantum oscillator gap energies for each mode are parenthesized.

$$CO_2(0,0,1) + CO_2(0,0,1) \rightarrow CO_2(0,0,2) + CO_2(0,0,0). \tag{4}$$

The vibrational transfer between the *different* modes (V-V′ or nonresonant transfer) is less efficient, having the typical transfer rates several times lower, according to [30].

In addition to the above-mentioned reactions, the various two- or three-body collisional processes leading to O atom recombination (some of them are exothermic) may also be important for the total energy balance in the O-containing discharges. These processes may involve both ground state (^{3}P) as well as the first excited (^{1}D) state of atomic oxygen, as well as the other states [31]. Among the typical examples are:

$$O(^1D) + O_2 \rightarrow O(^3P) + O_2, \tag{5a}$$

$$O(^3P) + O(^1D) \rightarrow O(^3P) + O(^3P), \tag{5b}$$

$$O(^3P) + O(^3P) + O_2 \rightarrow O_2 + O_2(X,0), \text{ etc.} \tag{5c}$$

2.2. The parameters defining CO_2 conversion

The CO_2 conversion efficiency in the discharge (as a result of CO_2 dissociation following by O^- recombination) is usually determined as a ratio between the densities of the decomposed CO_2 molecules to their initial density:

$$\chi = \frac{[CO_2]_{dec.}}{[CO_2]_{init.}}, \tag{6}$$

where $[CO_2]_{dec.}$ and $[CO_2]_{init.}$ refer to the decomposed and initial CO_2 molecular density, respectively. Let us note that in the pure CO_2 case, χ can be defined simply as $[CO]/[CO_2]_{init.}$, where [CO] is the density of CO molecules produced.

At the same time, the energy efficiency η is normally defined via the enthalpy of CO_2 dissociation ($\Delta H_{CO_2} = 2.9$ eV) and the energy spent for production of one CO molecule (E_{CO}) [6]:

$$\eta = \frac{\Delta H_{CO_2}}{E_{CO}}. \tag{7}$$

In a general case, both χ and η quantities are defined locally, as the supplied energy might be different depending on the point of interest in the discharge. Combining last two expressions and defining the specific energy input (SEI) as the energy delivered per a single CO_2 molecule in a certain discharge volume (usually expressed in eV or eV/molec), the energy efficiency yields:

$$\eta = \chi \ \frac{\Delta H_{CO_2}}{\mathrm{SEI}}. \tag{8}$$

The specific energy can be usually determined via the power P applied to the discharge and the flux of the gas F in the discharge tube:

$$\mathrm{SEI} = \frac{P}{F}\ , \ \text{or using more convenient units,}\ \ \mathrm{SEI(eV/molec)} = 0.014\ \frac{P(\mathrm{W})}{F(\mathrm{slm})}, \tag{9}$$

where P is in Watts and F is in slms (slm stands for standard liter per minute).

2.3. The main energy transfer channels in CO_2 plasma

In molecular plasma, the interaction between translational, rotational, and vibrational degrees of freedom, involving also the plasma electrons, leads to formation of the numerous energy exchange (relaxation) channels responsible for excitation or depletion of the corresponding energy subsystems. Some of these channels are especially important for understanding of the plasma-assisted CO_2 decomposition, due to the crucial role of the vibrational excitation in this process. Among them are the translational-translational (T-T), rotational-translational (R-T), as well as the e-V, V-V, and V-T channels mentioned above. The physical nature as well as the corresponding characteristic times for these energy relaxation mechanisms are described below.

2.3.1. T-T and R-T energy transfer

The T-T energy transfer is responsible for gas thermalization (i.e., establishing kinetic gas temperature). The characteristic time of this process can be estimated via the mean free path of the gas atoms and molecules and their mean velocity, being typically in the μs range for the gas pressure of several Torr and gas temperature of several hundred degree K. The R-T process, on the other hand, shows how fast the rotational degrees of freedom in molecular gas will be in the equilibrium with the translational (kinetic) motion of the gas particles. In order to estimate the characteristic time of this process, the model proposed by Parker [32] can be used (see Ref. [6] for further details). According to this model, the characteristic time of the R-T process can be determined based on the number of collisions necessary for equilibrium

between the rotational and translational degrees of freedom in discharge. The estimation of this time (for variety of gases) at about 20 Torr of the gas pressure leads to the values $\tau_{R-T} < 0.1$ μs, so the R-T equilibrium can be considered nearly instantaneous in the time scale related to this work, as compared below.

2.3.2. e-V energy transfer

For the efficient plasma-based molecular decomposition in the most low-temperature discharge cases, an efficient transfer of the electron energy to the vibrational degrees of freedom of the corresponding molecules is critical. In the case of CO_2, the characteristic time of this process can be determined through the corresponding rate coefficient k_{e-V} as

$$\tau_{e-V} \sim (k_{e-V} \cdot n_e)^{-1}, \tag{10}$$

where n_e is the electron density in plasma. Assuming that the electron density in the microwave discharge in the considered gas pressure range is about 10^{12}–10^{13} cm^{-3} [33], and taking $k_{e-V} \approx 10^{-8}$ cm^{-3}/s [34] corresponding to excitation of the lowest CO_2 vibrational level, we obtain τ_{e-V} ~10–100 μs. As we can see, under our conditions this process is much slower than the R-T energy relaxation.

2.3.3. V-V energy transfer

The rate of establishing vibrational equilibrium within each vibrational mode of a certain molecule is defined by the V-V energy transfer and the corresponding characteristic time. In the case of CO_2 molecule, the V-V rates are roughly comparable for all three vibrational modes (see **Figure 2**) having the differences within the order of magnitude [30]. A rough estimation of the V-V characteristic time for the asymmetric mode of CO_2 gives

$$\tau_{V-V} = (k_{V-V} \cdot [CO_2])^{-1} \sim 3 \text{ ns, (at 20 Torr and 300K)}, \tag{11}$$

where k_{V-V} is the corresponding rate coefficient ($k_{V-V} \sim 5 \cdot \times 10^{-10}$ cm^{-3}/s for the first energy levels of the asymmetric mode, according to Ref. [6]), and $[CO_2]$ is the ground state number density of CO_2 molecules in the discharge estimated in our case using the actual values of the gas pressure and temperature. As we can see that the V-V process is nearly instantaneous being faster than both R-T and e-V processes.

2.3.4. V-T energy transfer

While the plasma electrons transfer their energy to the CO_2 vibrational modes, the vibrational excitation might be suppressed by the translational motion of gas particles, as a result of V-T energy transfer. This effect should be considered harmful for the efficient CO_2 decomposition, taking into account the importance of vibrational excitation in this case. The characteristic time of the V-T process, τ_{V-T}, varies significantly spending on the gas pressure and gas temperature and can be estimated based on several models available elsewhere [5, 6]. One of them is represented by a semiempirical expression proposed by Millikan and White [35]:

$$\tau_{V-T} = \frac{1}{p} \exp\left[1.16 \cdot 10^{-3} \mu^{\frac{1}{2}} (\hbar\omega)^{\frac{4}{3}} \left(T_0^{-\frac{1}{3}} - 0.015\mu^{1/4}\right) - 18.42\right], \quad (12)$$

where τ_{V-T} is the relaxation time (s), p is the gas pressure (atm), T_0 is the gas temperature (K), μ is the reduced mass of the colliding molecules (a.m.u.), and $\hbar\omega$ is the vibrational gap for the corresponding vibrational mode (also expressed in K). The expression (12) is very sensitive to the gas temperature as well as to the vibration mode under consideration, giving extremely long characteristic times for the CO_2 asymmetric mode (~10^5 s). This might be related to the fact that this expression describes well only the first (lowest) vibrational states of the CO_2 bending mode, for which (at 20 Torr and 1000 K) the estimates give $\tau_{V-T} \approx 15$ μs, whereas at 300 K this value increases to about 150 μs.

The role of the gas temperature in the V-T energy transfer is additionally illustrated in **Figure 3**, where the τ_{V-T} time is calculated in the 300–3000 K temperature range. The calculations clearly show that τ_{V-T} can vary by nearly two orders of magnitude in the mentioned temperature

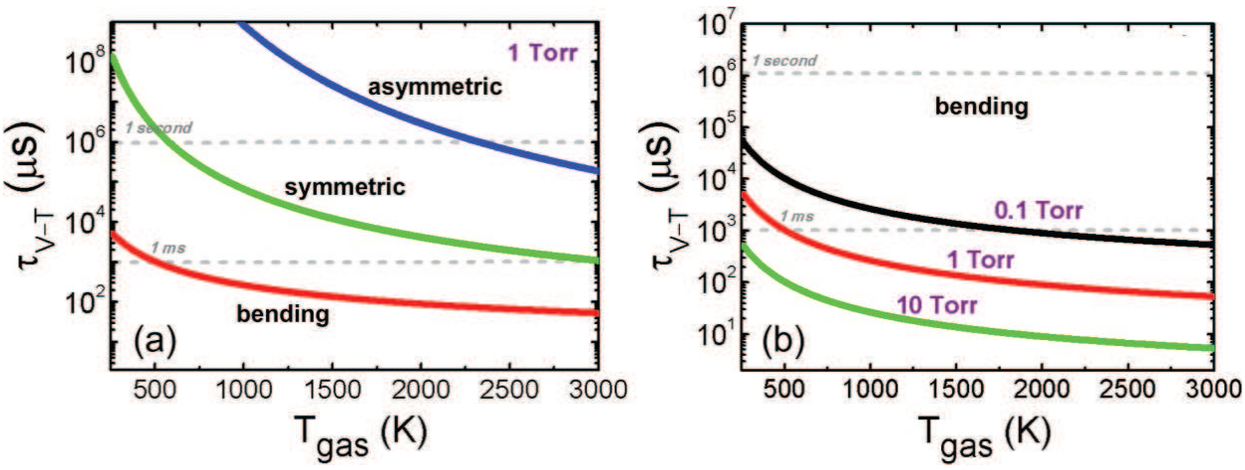

Figure 3. The characteristic time of V-T relaxation as a function of gas temperature calculated (based on Ref. [35]) for three vibrational modes of CO_2 at 1 Torr (a), and for the bending vibrational mode at different gas pressure (b).

Process	Characteristic time (at 20 Torr)	Comment	Source
T-T	<0.1 μs	$T_{gas} = 300$ K	[36]
R-T	<0.1 μs	$T_{gas} = 300$ K	[6, 32] **
e-V *	~10 μs	$T_e = 1.5$ eV, $n_e \sim 10^{13}$ cm^{-3}	[34, 37] **
V-V	<0.01 μs	$T_{gas} = 300$ K	[6]
V-T (bending)	150 μs	$T_{gas} = 300$ K	[6, 35] **
V-T (bending)	15 μs	$T_{gas} = 1000$ K	[6, 35] **

* Done for the symmetric stretch and bending CO_2 vibration modes: (1,0,0) and (0,1,0).
** In case of multiple literature sources the results are averaged.

Table 1. The estimates for the characteristic time of the main energy transfer processes described in the Section 2.3.

range. The calculations also point out on a primary role of the CO_2 bending mode in this process, as the one corresponding to the fastest V-T transfer (see **Figure 3(a)**). Naturally, the τ_{V-T} time is inversely proportional to the gas pressure since the number of collisions per unit time defining the V-T energy exchange rate is directly proportional to pressure (see **Figure 3(b)**).

The rough estimates for the characteristic times corresponding to the main energy exchange processes described in this section are summarized in **Table 1**.

3. The experimental

3.1. The plasma sources used

The pulsed microwave discharges (surfaguide-type) have been used as the plasma sources in this study. In these discharges, plasma is sustained by an electromagnetic wave with the filling frequency in the microwave range (either 0.915 or 2.45 GHz in our case) coming out of two orifices in the surfaguide [38], as schematically shown in **Figure 4**. In our case, the electromagnetic radiation has been modulated by the nearly square pulses with the repetition frequency ranging from 0.5 to 30 kHz. The duty ratio of the pulses was kept equal to 50%. The discharges were sustained in the quartz tubes (14 mm in diameter and 31 cm long) in which the gas flow has been regulated by digital mass flow controllers. Each quartz tube was additionally cooled by a flow of Si oil (~2 l per minute) having the temperature of about 5°C (in the 0.915-GHz system) or 10°C (in the 2.45-GHz system). The total gas flow rate has been varied in the range from about 0.08–2.7 slm. Both pure CO_2 and CO_2 + 5% N_2 gas mixtures have been utilized. The time-averaged power applied to the discharge was always fixed at the level of either 0.4 kW (2.45-GHz system) or 1.0 kW (0.915-GHz system). The reflected electromagnetic radiation has been minimized in each plasma source using three-stub automatic tuning systems.

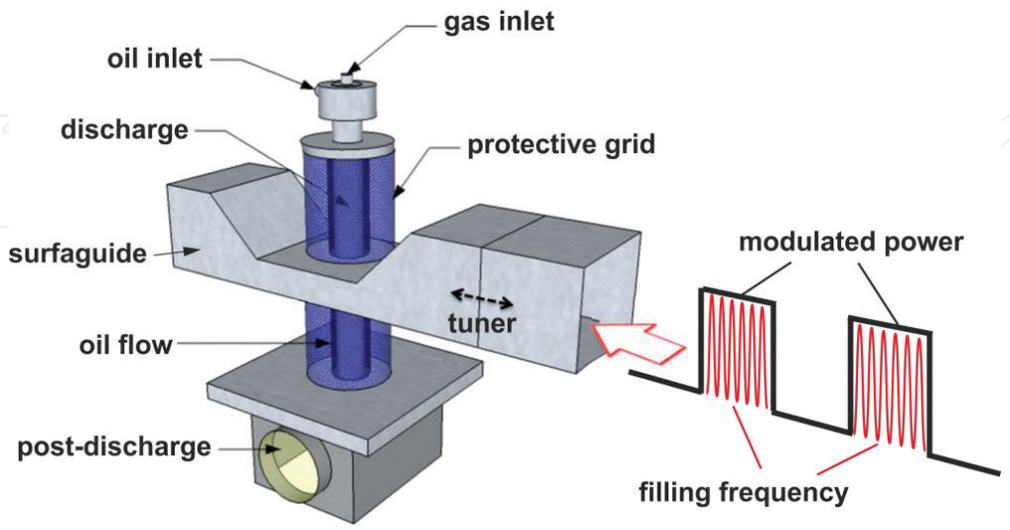

Figure 4. The illustration of the surfaguide microwave discharge system. The modulation of the initial electromagnetic wave (filling frequency of either 2.45 GHz or 0.915 GHz) by the kHz pulses is shown schematically.

The reflected power was always around 5% for 2.45-GHz system, and totally negligible (presumably <1%) in the case of 0.915-GHz system. Further experimental details related to the mentioned microwave systems can be found elsewhere [15, 39]. The diagnostics of the microwave discharge has been undertaken both in the discharge active zone (i.e., near the waveguide excitation point) and in the postdischarge (at about 40 cm below the plasma excitation point), as described in the following section.

3.2. The diagnostic techniques used

3.2.1. Diagnostics in the discharge zone

Optical emission spectroscopy (OES), including emission actinometry and ro-vibrational analysis, has been applied for characterization of the CO_2 conversion efficiency as well as the gas temperature in the discharge zone. Gas temperature has been also monitored by a thermocouple at the beginning of the postdischarge (i.e., about 17 cm below the excitation point). The rotational band from the CO Angstrom system corresponding to the $B^1\Sigma^+$ ($v' = 0$) – $A\ ^1\Pi$ ($v'' = 1$) optical transition has been used for the rotational temperature determination in the discharge. Gas temperature has been assumed equal to rotational temperature of CO molecules, based on the analysis undertaken elsewhere [15, 40].

In order to determine the CO_2 conversion efficiency in the discharge area, the optical actinometry method based on the addition of a small amount of molecular nitrogen (5% in our case) to the CO_2 gas has been applied. This method is based on the measurement of the emission lines ratio between the unknown species in the discharge (CO) and the known admixture (N_2). As a result, assuming corona excitation in the discharge volume, the absolute density of species of interest can be determined, as performed recently by Silva et al. [15]. The relative error of this method is supposed to be <10%, based on our estimations.

An Andor Shamrock-750 monochromator having 0.75 m of focal length and equipped with an Andor iStar-740 series intensified charge coupled device (ICCD) camera has been used for spectral acquisition in this work. The spectral resolution during the measurements was equal to about 0.05 nm (at 500 nm). The accumulative ICCD mode of the spectral acquisition has been used for all the measurements.

3.2.2. Diagnostics in the postdischarge zone

In the case of 2.45-GHz plasma source, the products of CO_2 dissociation (such as CO ground state molecules and O ground state atoms) have been detected in the postdischarge area using a two-photon absorption laser-induced fluorescence (TALIF) technique [41]. This technique is based on the laser excitation of the molecular or atomic species in the discharge or postdischarge by a simultaneous absorption of two laser photons, following by a spontaneous emission of light (fluorescence) corresponding to an optical transition between the upper (excited) state and the intermediate state. The spectral schemes using laser excitation at 225.6 nm (for O atom) or 230.07 nm (for CO molecule) following by the fluorescence at 844.7 nm (O) or 483.5 nm (CO) have been applied in this work [42, 43]. The summary of the corresponding spectral transitions used for O and CO detection by TALIF technique is given in **Table 2**.

Spectral parameter	Values	
Specie of interest	**O [42]**	**CO [43]**
Lower state	$O(^3P_2)$	$CO(X^1\Sigma^+)$
Upper (laser-excited) state	$O(^5P)$	$CO(B^1\Sigma^+)$
Energy gap	10.74 eV	10.78 eV
Laser excitation wavelength	225.6 nm	230.07 nm
Fluorescence wavelength	844.68 nm	483.50 nm
Bandpass filter used	840 nm	480 nm

Table 2. The spectral transitions for TALIF diagnostics of the ground state O and CO in the postdischarge of the 2.45 GHz MW source used in this work.

A Sirah dye laser working at 10 Hz of repetition rate and having 5 ns of the pulse duration pumped by a Spectra Physics YAG:Nd laser has been utilized for TALIF diagnostics. A Coumarin 450 dye solution (in ethanol) has been used in the dye laser. During the measurements, the laser pulses were not synchronized with the plasma pulses, thus giving the time-averaged values of the corresponding ground state densities in the postdischarge. The provided averaged values are supposed to reflect an overall system performance regarding CO_2 conversion, being especially interesting from the applications point of view.

Another type of diagnostics applied to the 0.915-GHz MW discharge was a gas chromatography (GC) technique. The GC technique is based on the different gas elution time on the analyzer walls, representing *ex-situ* time-averaged gas analysis, which has been used for characterization of various gas mixtures, including the products of the CO_2 decomposition [11]. In spite of being an *ex-situ* technique, GC provides the results that can be compared with the laser-based (*in-situ*) techniques for the stable dissociation products, which is valid for CO ground state molecules. In our case, a Bruker 450-GC gas chromatograph equipped with a sampling system has been used for the postdischarge characterization of the dissociation products in the 0.915-GHz MW source. In the described GC system, a low-pressure gas sample is diluted with carrier gas (argon) before its injection into the gas chromatograph for the further *ex-situ* analysis.

4. Optimization of CO_2 conversion in microwave plasma

4.1. The emission spectroscopy analysis

CO_2 decomposition in a flowing gas discharge can often be noticed visually by changing the color of the discharge before and after the excitation point (waveguide position) in the discharge tube. This corresponds to the formation of CO molecules in the so-called discharge "active zone" (being approximately 6 cm wide in our case, according to Ref. [15]), where the decomposition process is mainly taking place. In the case of CO, the observed emission

corresponds to the CO Angstrom band ($CO(B^1\Sigma^+)$ – $CO(A\ ^1\Pi)$) and partially to the third positive (3P) CO band ($CO(b^3\Sigma^+)$–$CO(a\ ^3\Pi)$) [44], as shown in **Figure 5**. In the CO_2-N_2 gas mixture, these effects are qualitatively similar to the pure CO_2 case. The O atom emission triplet around 777 nm is also clear in both cases, whereas the N atom emission around 821 nm is rather negligible in the case of N_2 admixture, as shown in **Figure 5(b)**.

The emission spectra corresponding to the CO_2-5%N_2 gas mixture and taken in a wider spectral range are presented in **Figure 6**. As we can see that at higher gas pressure, a much stronger contribution of the N_2 and N_2^+ molecular bands such as N_2 second positive band ($N_2(C\ ^3\Pi_u)$-$N_2(B\ ^3\Pi_g)$), N_2^+ first negative band ($N_2^+(B^2\Sigma_u^+)$-$N_2^+(X^2\Sigma_g^+)$), and N_2 first positive band ($N_2(B\ ^3\Pi_g)$-$N_2(A^3\Sigma_u^+)$) is evident. The contribution of the CO Angstrom ro-vibrational band is rather strong in both cases. The structure of all the observed CO rotational

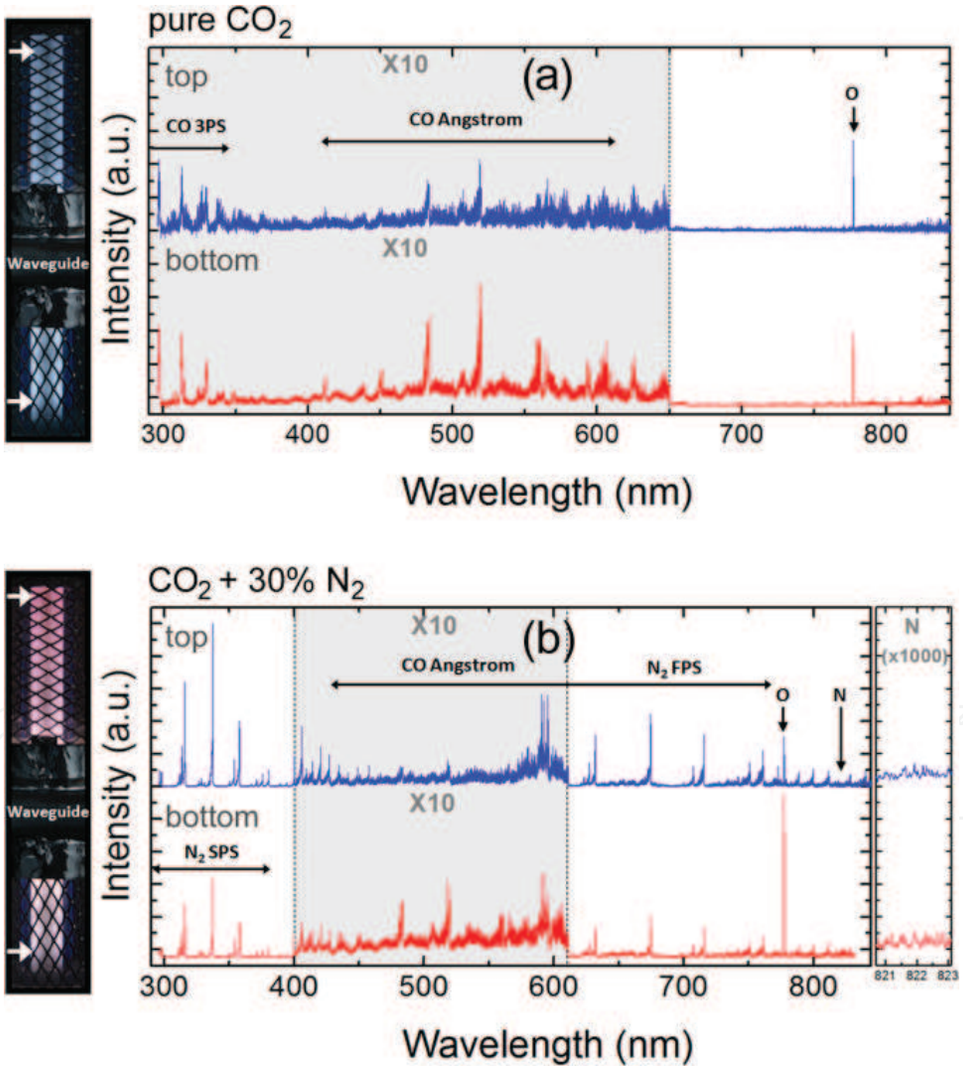

Figure 5. Time-averaged emission spectra measured in the 2.45-GHz MW discharge at two different special positions for pure CO_2 (a) and CO_2 + 30%N_2 mixture (b). Gas pressure is about 2 Torr. Bold arrows indicate the top and bottom measurement points. The spectral correction is applied in both cases. The corresponding discharge photographs are shown on the left side.

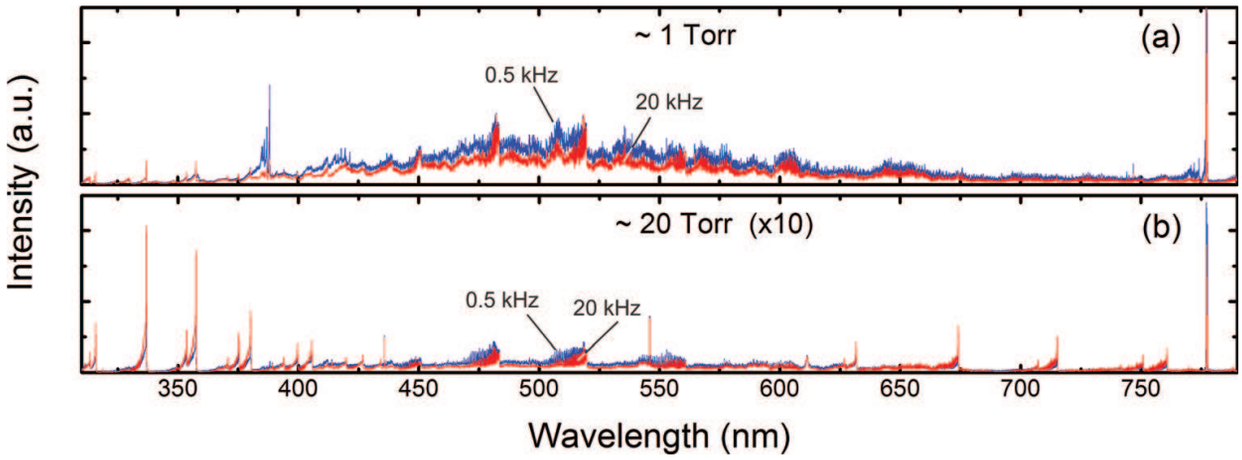

Figure 6. Time-averaged emission spectra taken in the 2.45-GHz MW discharge at high and low plasma pulse frequency at 1 Torr (a) and ~20 Torr (b) in the $CO_2 + 5\%N_2$ gas mixture. No spectral correction is applied.

bands is different at high and low pulse repetition frequency. At low frequency, they are more elongated toward the shorted wavelengths corresponding to higher gas temperature in the discharge, confirmed by calculations, whereas the gas temperature is essentially lower at high frequency.

In addition, the low pressure spectra possess much more pronounced continuum band in the 400–600 nm range (**Figure 6(a)**). Such a strong contribution of the continuum band is likely related to the chemiluminescence induced by the CO–O recombination process, as also detected in Ref. [15] and analyzed in Refs. [45, 46].

4.2. CO_2 conversion efficiency and related results

The main results on the CO_2 conversion efficiency (χ) and energy efficiency (η) are described in this section aiming at comparison of two mentioned MW plasma sources. The obtained data are presented as a function of the plasma pulse repetition frequency (f) aiming at the clarification of namely the effect of plasma power modulation on the CO_2 conversion.

The relative density of the CO ground state molecules detected by the TALIF technique in the postdischarge of the considered MW plasma sources is shown in **Figure 7**. The beneficial effect of power modulation is evident in this case leading to a fourfold increase in the CO density (so the corresponding CO_2 conversion efficiency) at low pulse frequency. The maxima of χ are observed at about 0.5 kHz (for the 2.45-GHz system) and at about 0.8 kHz (for the 0.915-GHz system). Apart from the different positions of these maxima, in the 2.45-GHz case, maximum appears to be much narrower than that detected in the 0.915-GHz discharge case.

As also clear from **Figure 7(a)**, the O production is strongly suppressed at low pulse frequencies (below 1 kHz), when the dissociation of CO_2 reaches its maximum. At the same time, the O_2 density also has a maximum at low frequency (detected in the 0.915-GHz system though), pointing out on the efficient O-recombination process under these conditions (see Figure 7(b)). Note that the CO and O_2 densities determined by GC are not different by a factor of two in this

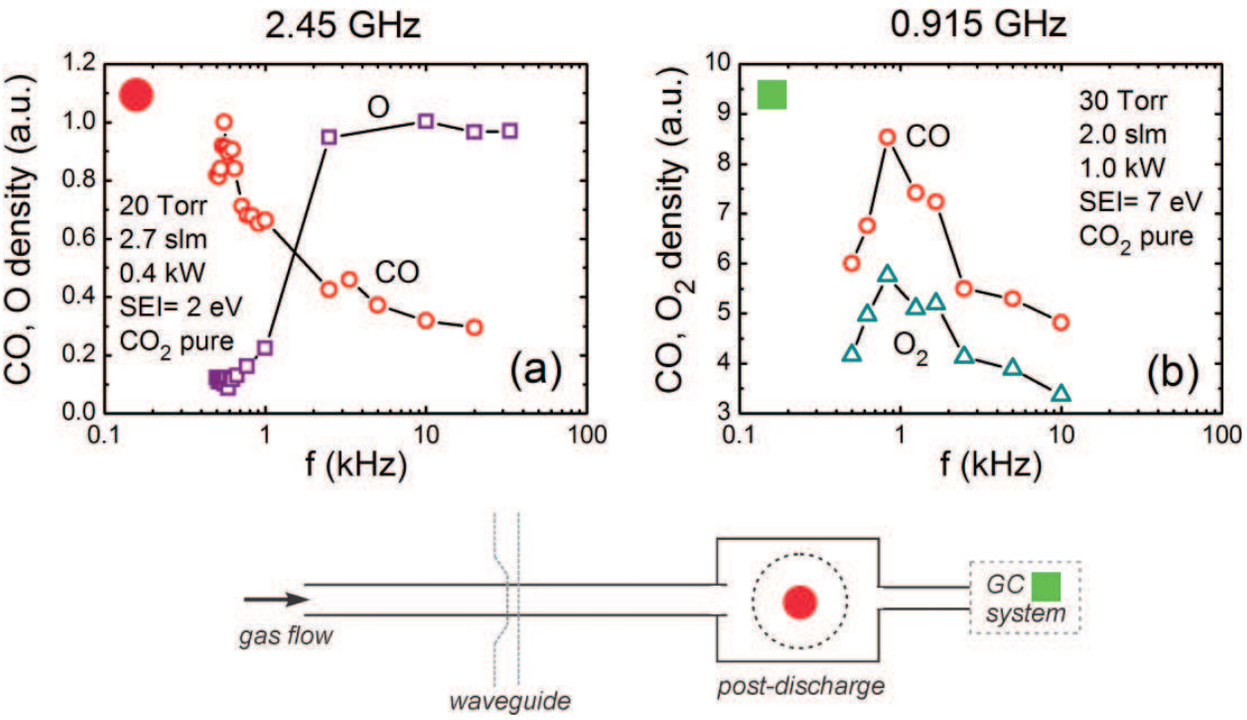

Figure 7. (a) Normalized density of CO and O in the postdischarge as a function of the plasma pulse repetition frequency (f) measured by the TALIF technique in the 2.45-GHz MW system. (b) The relative density of CO and O_2 molecules measured in the 0.915-GHz MW system by GC. The points of measurement are indicated below.

case, due to the fact that calibration of our GC system response was not performed. Finally, the CO density decay slopes measured in two different plasma sources reveal rather similar behaviors.

The data on the CO_2 conversion efficiency as a function of the plasma pulse frequency determined by optical actinometry in the 2.45-GHz system (in the discharge area) and by GC in the 0.915-GHz system (in the postdischarge area) are compared in **Figure 8**. As we can see that there is a fourfold difference between the observed maximum values of χ in these two cases. This is related to the power differences between the considered plasma sources as well as to the fact that the actinometry measurements were performed in the center of the discharge tube where the CO_2 conversion is not yet fully accomplished. After the corresponding corrections, the obtained conversion efficiency values appear to be very similar for both systems. The energy efficiency values corresponding to the observed χ maxima in this case are 0.14 and 0.16, respectively. In addition, in the case of **Figure 8(a)**, the CO_2 conversion curve does not reveal a clear maximum at low plasma pulse frequency, which is only present in the 0.915-GHz case (**Figure 8(b)**). This phenomenon might be related to the gas displacements in the discharge tube, as well as to the differences in the discharge geometry. The physical reasons for the observed behavior of χ and CO production in the postdischarge are discussed in the following section.

An interesting behavior of the gas temperature in the discharge tube along the gas flow direction has also been detected, as a result of combination of ro-vibrational spectral analysis and

http://dx.doi.org/10.5772/67875

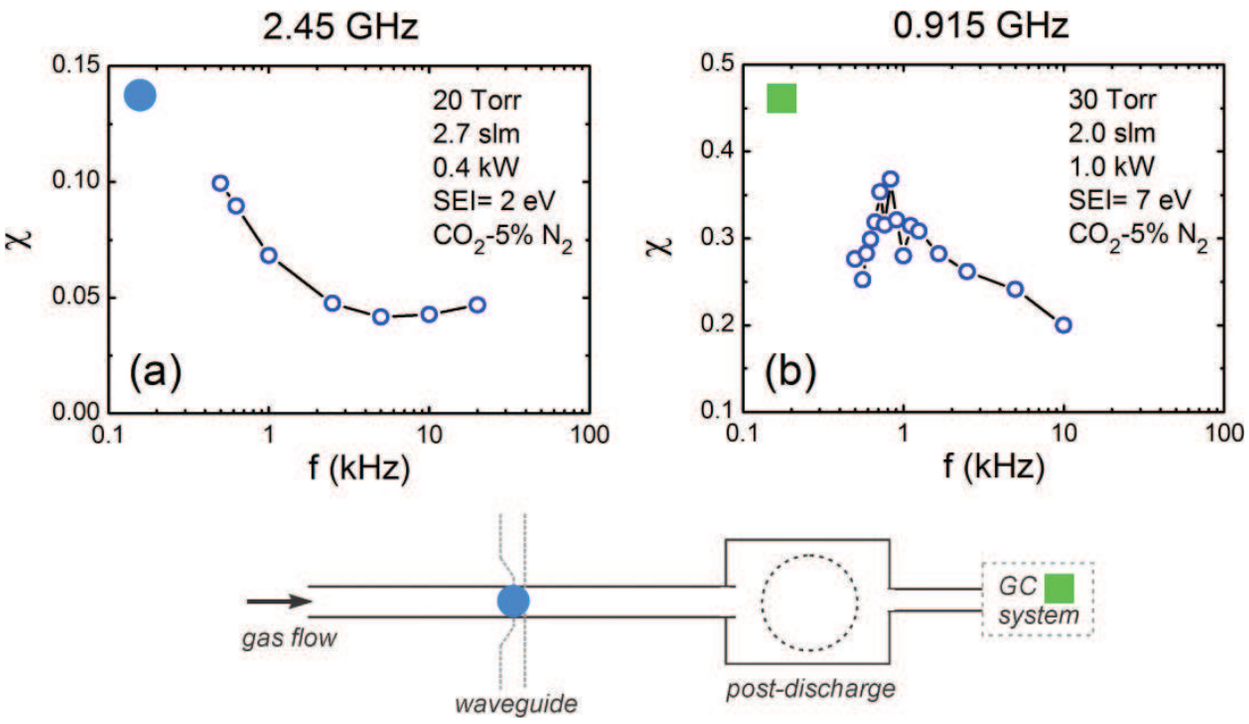

Figure 8. The CO_2 conversion efficiency χ as a function of the plasma pulse repetition frequency (f) measured in the discharge region of the 2.45-GHz MW system by optical actinometry (a), and in the postdischarge region of the 0.915-GHz MW system by GC (b). The energy efficiency corresponding to the maximum χ values is equal to 0.14 (a) and 0.16 (b). The points of measurement are indicated below.

thermocouple measurements. The corresponding results are shown in **Figure 9**. The gas temperature in the discharge zone has been measured in this case using the rotational band of CO, following by the Boltzmann plot approximation for the obtained rotational populations, as described elsewhere [15, 47]. As a result, the error bars in **Figure 9(a)** correspond to the error of Boltzmann fit applied to the rotational distributions for each data point.

As we can see that a trend for CO_2 conversion efficiency shown in **Figure 8(a)** clearly correlates with the one obtained for the gas temperature in the discharge zone, shown in **Figure 9(a)** for the 2.45-GHz MW source (the point of measurements is indicated by a dot). At the same time, at the end of the discharge tube (indicated by a square), the temperature behavior is roughly opposite. In this case, the gas temperature is somewhat reduced at low plasma pulse frequencies (see **Figures 9(b)** and **9(c)**). The observed temperature reduction is especially clear in the case of 0.915-GHz plasma source, when the gas temperature drops by nearly 200 K at low pulse frequency. In this case, we can talk about the existence of a temperature gradient established between the excitation point in the discharge and the end of the discharge tube (beginning of the postdischarge). Apparently, this gradient is much larger at low pulse repetition frequencies (about 600 K in our case, based on **Figure 9(a)** and **9(b)**) compared to the high frequency (only about 300 K). Based on the data shown in **Figure 9(c)**, one can speculate that this effect might be also similar in the 0.915-GHz plasma source case (for which the T_{gas} data in the discharge area are not available).

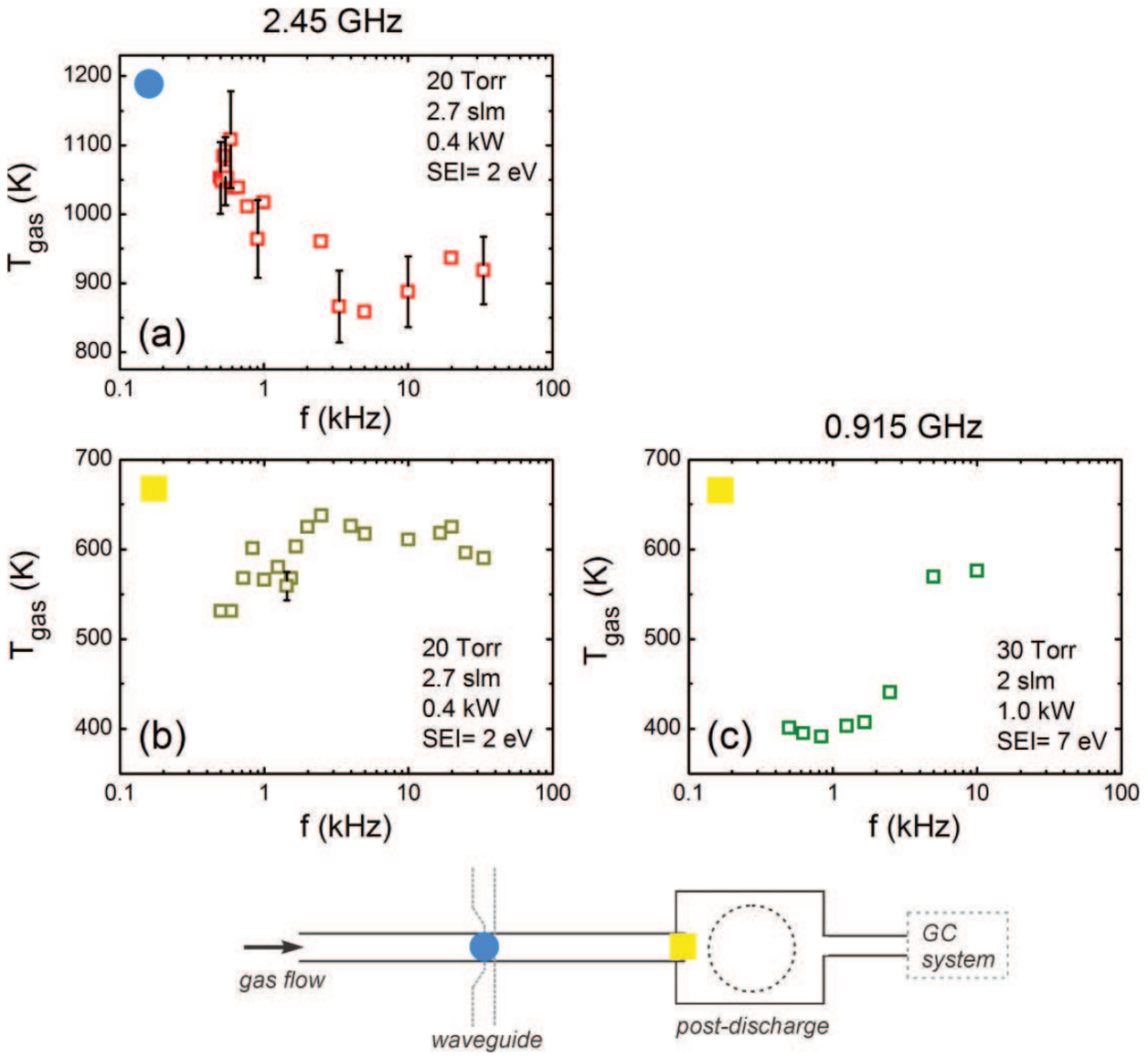

Figure 9. The evolution of the gas temperature as a function of plasma pulse repetition frequency (f) measured in the discharge area (a) and at the end of the discharge tube (b) in the 2.45-GHz MW system, as well as at the end of the discharge tube in the 0.915-GHz MW system (c). Pure CO_2 gas is used. The points of measurement are indicated below.

4.3. Discussion

Several physical effects should be taken into account for proper explanation of the observed CO_2 conversion efficiency as a function of the plasma pulse frequency, as well as its relation to the measured gas temperature, both in the discharge and the postdischarge areas. Among the main physical phenomena responsible for the efficient molecular decomposition, the vibrational excitation of CO_2 molecules, the gas displacement in the tube, as well as V-V and V-T relaxation processes in the discharge should be considered. The CO rotational temperature, at the same time, being determined using a CO rotational emission band, is supposed to be an indicator for the other important processes in the discharge, such as V-T energy transfer. This temperature is supposed to be in equilibrium with the kinetic gas temperature rather quickly

(μs scale) as a result of the fast R-T transfer, according to our estimations (see **Table 1**), giving nearly instantaneous image of the gas heating.

According to our estimations, the plasma electrons transfer their energy to the (lowest) CO_2 vibrational states during the time $\tau_{e-V} \sim$ 10–100 μs. This time might be somewhat smaller at higher gas pressures, as one may expect a slight increase in n_e in this case [33]. At the same time, the equilibration of the vibrational distributions for each vibrational mode is taking place nearly instantaneously, with a time constant in the order of magnitude of 0.01 μs or less, estimated for our discharge conditions. Finally, the loss of the vibrational excitation as a result of vibrational energy transfer to the translational gas motion through the bending vibrational mode (resulting in gas heating) takes place with a characteristic times ranging roughly between 15 and 150 μs in our case, depending on the gas temperature. Let us also note that the V-T energy exchange occurs faster in the discharge active zone, where the gas temperature may exceed 1000 K (thus $\tau_{V-T} <$ 15 μs), and slower in the other parts of the discharge when the temperature might be close to the room temperature ($\tau_{V-T} \sim$ 150 μs).

The gas velocity (i.e., gas displacement) in the tube is another key parameter defining the residence time for CO_2 molecules in the discharge active zone (~6 cm wide in our case). The rough estimations for the gas velocity based on the ideal gas low give the values of about 40 m/s in the 2.45-GHz source case (at 20 Torr, 1100 K, and 2.7 slm of a total gas flow), and about 30 m/s in the 0.915-GHz case (at 30 Torr, 1600 K [48], and 2 slm of a total gas flow).

Taking into account the above-mentioned estimations, the observed processes along the gas flow direction can be explained as follow. At first, in the discharge zone (the excitation point), the CO_2 vibrational excitation is initiated by the fast e-V energy transfer. The e-T and T-T energy exchange channels, at the same time, may contribute to the overall gas heating. In addition, the gas heating due to the V-T transfer should also occur, which is supposed to be more efficient at longer plasma off-times (i.e., at low frequencies). Even though the V-T characteristic time is rather short according to our estimations (~15 μs at 1000 K), its contribution at lower pulse repetition frequency is supposed to be more pronounced, likely resulting in the increase of gas temperature at low frequency measured in our case (see **Figure 9(a)**). Note that the gas temperature has been determined in this work based on the time-average spectral data and the time-resolved measurements may be necessary for a full clarification of the temperature evolution. The additional experiments [49] indicate that the vibrational temperature of the $N_2(X)$ ground state molecules in the active zone decays rapidly under the increase of the pulse repetition frequency, following the trends obtained for CO density (**Figure 7(a)**) and CO_2 conversion (**Figure 8(a)**). Rather fast nonresonant V-V′ energy exchange taking place between N_2 and CO_2 (see Ref. [50] and refs therein) leads to similar expectations for the CO_2 vibrational temperature as well. This leads to a conclusion that vibrational excitation is the main reason for higher CO_2 dissociation at low pulse frequency, in spite of the fact that the V-T transfer is also enhanced in this case (gas temperature increase is observed). A gradual decay in the CO_2 dissociation (**Figure 8**) leading to a weaker CO production (**Figure 7**) at high frequencies is most probably related to a less efficient e-V transfer at shorter plasma pulse durations. The top estimations of the e-V transfer time in our case correspond to the pulse frequency of about 5 kHz, only roughly correlating with the obtained data still requiring final clarification first of all based on the precise measurements of the electron density in the discharge active zone.

The presence of maximum in the frequency dependences of χ (0.915-GHz case, **Figure 8**) and CO density in the postdischarge (**Figures 7** and **8(b)**) at low pulse frequencies deserves special attention, since the gas displacement in the tube may play a decisive role in this effect. Three cases can be considered explaining the observed data, namely: (i) a slow gas displacement, when the gas displacement is small between two consecutive plasma pulses, (ii) a "resonant" gas displacement, when the gas displacement time in the active zone is almost equal to the plasma pulse duration, and (iii) a fast gas displacement, when the gas displacement time is shorter comparing to the time between two plasma pulses. Since in our case, the gas velocities are comparable for both the 2.45-GHz (~40 m/s) and 0.915-GHz (~30 m/s) systems, it can be shown that nearly the resonant case is realized at low plasma pulse frequency (0.5 kHz) in both systems. This results in a nearly maximum system performance in terms of CO_2 decomposition and energy efficiency. More pronounced χ-maximum found in the 0.915-GHz case, as well as its position shifted toward higher plasma pulse frequency values may be a result of the differences in system geometry as well as the errors related to gas pressure and especially gas temperature determination, which are the critical parameters for gas velocity.

We should note that at lower pulse frequencies (or higher gas flows) one may expect a significant drop in the CO_2 decomposition, as the fast gas displacement limit will be achieved and some portions of the passing gas will remain untreated by plasma. On the other hand, at higher pulse frequencies, as observed in our case, a considerable drop in the CO_2 conversion should be likely explained by a combination of several factors, such as (i) a decrease of the e-V transfer contribution at shorter pulse durations, (ii) a decrease of the role of dissociative recombination of CO_2^+ (via the reaction: $e + CO_2^+ \rightarrow CO + O$, see Ref. [29]) in this frequency range, as suggested by Silva et al. [49], (iii) decomposition of CO molecules in the active zone when residence time is too long. The third argument, however, is supposed to play a minor role, due to the synchronous changes of both CO and O_2 densities observed in the postdischarge detected by GC, as shown in **Figure 7(b)**.

Finally, some attention should also be given to the gas temperature differences in the excitation point and at the beginning of the postdischarge, as well as to the corresponding temperature gradient between these points. At low plasma pulse frequency, the high values of both gas temperature and CO_2 conversion are observed, whereas the O ground state density reaches its minimum. The gas temperature at the beginning of the postdischarge is rather low in this case, resulting in a high temperature gradient between the tube center and its end. At high frequency, on the other hand, CO_2 conversion drops several times, along with the CO density, measured in the postdischarge. The O ground state density in the postdischarge is roughly 10 times higher in this case (see **Figure 7(a)**). Also, the gas temperature is getting lower in the discharge area and higher in the postdischarge (comparing to the low frequency case), flattening the mentioned temperature gradient.

Based on our experimental data, the observed gas temperature phenomena may be explained by the O atom recombination. Considering two main ways of this recombination, namely the reaction (2) and reactions (5) mentioned above, we can conclude that at low frequency ground state, O gets efficiently recombined either with $CO_2^{vibr.}$ or with atomic/molecular oxygen. The additional heat released as a result of (some) recombination processes (along with the e-T energy

transfer) is a probable reason for the gas heating in the discharge area. As a result of the efficient O-recombination, the delivery of ground state O to the postdischarge is significantly reduced in this case, the corresponding heat release is reduced as well, resulting in a low temperature. On the other hand, at high pulse frequencies CO production drops (partially due to the reduced O-CO_2^{vibr} recombination), letting more O ground state atoms to be formed as a result of electron impact dissociation in the discharge area and to be transported to the postdischarge. The O-recombination processes, other than O-CO_2^{vibr} one, are still taking place all the way down to the postdischarge, thus "blurring" the hear release along the discharge tube and flattening the temperature gradient between the excitation point and the end of the tube. The O-O recombination on the termocouple surface might also be an important factor contributing to the observed tempearture elevation in this case.

The given explanation, however, describes the observed temperature behavior only in the first approximation, do not taking into account numerous additional O-recombination reactions, e.g., those involving excited O states (such as O(^{1}D) state), as well as the processes in which O ions are involved (such as $O^+ + O_2(a) \rightarrow O_2^+ + O(^3P)$ or $O^+ + O^- \rightarrow O(^3P) + O(^3P)$, see Ref. [31]), which may additionally contribute to the O ground state density distribution along the discharge tube, as a result of quenching of the excited O states. The reactions (5a) and (5b) mentioned above also correspond to this case. This described temperature effects may still need a further clarifications in the future, based on the kinetic discharge modeling. It is already clear, however, that these effects may play a key role for the future optimization of the plasma-based CO_2 conversion in the microwave gas-flowing discharges, since by lowering the gas temperature the lifetime of CO_2 vibrational excitation might be significantly enhanced, which is favorable for efficient CO_2 conversion.

4.4. Comparing with literature

In this section, the most prominent results obtained based on the power modulation in the pulsed microwave plasma considered in this work are compared with the available literature data. The most competitive literature results have been chosen for this purpose, representing microwave, DBD, and gliding arc discharges. The discharges operating with catalysis, i.e., using a plasma-catalyst synergy, are not considered (except for one example). The corresponding data are summarized in **Figure 10**.

As we can see, the most competitive results are grouping around the diagonal line corresponding to the value of SEI of 2.9 eV/molec, as the virtual limit of the CO_2 conversion (when $\chi = \eta = 1$) can be reached only in this case. The beneficial effect of the plasma power modulation (indicated by solid arrows) resulting in about twofold increase of the CO_2 conversion and energy efficiencies is evident for both microwave plasma sources described in this chapter. In addition, the effect of plasma catalysis studied by Chen et al. [28] in the 0.915-GHz source is also given for illustration (indicated by dashed arrow). More than a twofold gain for both χ and η values has been achieved in this case.

Considering the other discharge types, the most promising results on the CO_2 conversion have been obtained so far in an atmospheric DBD discharge using the effect of power modulation (open square in **Figure 10**), thus one more time underlining significance of this effect for better

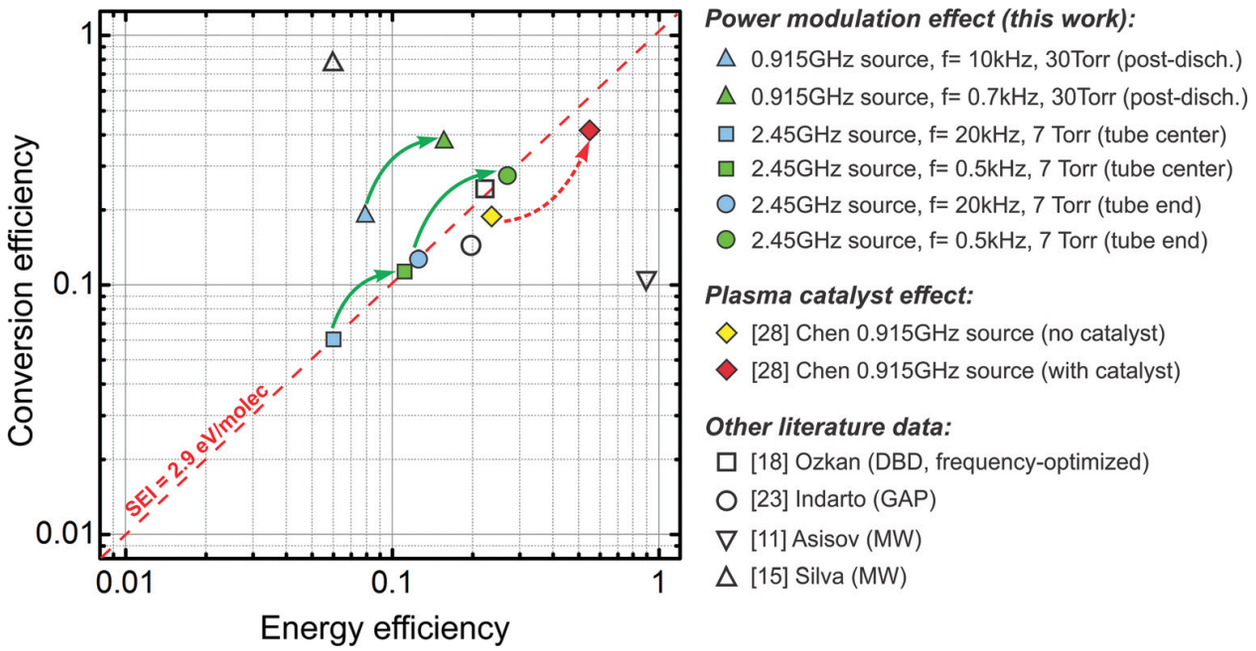

Figure 10. The optimized values of the CO_2 conversion efficiency (χ) and energy efficiency (η) obtained in this work in both the 2.45-GHz and 0.915-GHz plasma sources and compared to the most competitive literature data. The gain obtained by the power modulation and the catalysis effects in our case is indicated by solid and dashed arrows (respectively).

plasma-assisted CO_2 conversion. Somewhat lower conversion efficiency has been achieved in an atmospheric GAP case, as studied by Indarto et al. [23] (open circle). On the other hand, two other examples related to the low-to-moderate pressure microwave discharges, one representing high conversion efficiency, but rather low energy efficiency attained as a result of applying high SEI [15] (open up-triangle), and the other representing the well-known work of Asisov et al. [11] where a supersonic gas flow enabled high energy efficiency (open down-triangle). These two examples are shown in order to illustrate the well-known χ-η tradeoff, especially evident in the nonoptimized discharge cases. In this regard, the results presented in this work clearly demonstrate the importance of the discharge tuning, as one of the possible ways to partially overcome this tradeoff, simultaneously achieving high conversion and energy efficiencies of CO_2 conversion.

5. The perspectives

Based on the obtained experimental results as well as on the comparison with the literature data, it is clear that there is a definite room for further improvement of the CO_2 conversion in low-temperature microwave plasma. It should be noted that the improvements achieved by tuning only the plasma parameters, without changing the energy expenses in the whole system, are implied in this case. The beneficial effect of modulation (i.e., timely interruption) of the electric power delivered to the discharge is already evident based on the results described in this chapter. At the same time, there are still few physical parameters that should

be considered critical for the further maximization of the plasma-assisted CO_2 conversion. The main factors influencing these improvements are summarized in **Figure 11**, and can be subdivided into three following groups:

- Power-related parameters
- The parameters related to gas mixture and gas dynamics
- Plasma catalysis

Among the power-related parameters, the plasma pulse duty ratio, as well as the gas residence time (related to the gas velocity in the discharge as well as to the gas pumping speed in the whole system), requires deeper investigation. One may expect an essential improvement of the CO_2 conversion efficiency as a result of more careful optimization of the gas residence time in the active zone, along with the optimization of the plasma pulse duty ratio, in order to fully utilize the resonant effects related to the relevant energy transfer processes described in this work.

The second group includes the gas mixture control as well as the gas flux optimization including gas expansion effects. The influence of the gas mixture in the microwave plasma has already been studied recently showing a beneficial effect for CO_2 decomposition [14]. The optimization of the gas flux dynamics, e.g., via the gas expansion for the sake of lowering kinetic gas temperature, on the other hand, represents a powerful way to control the V-T

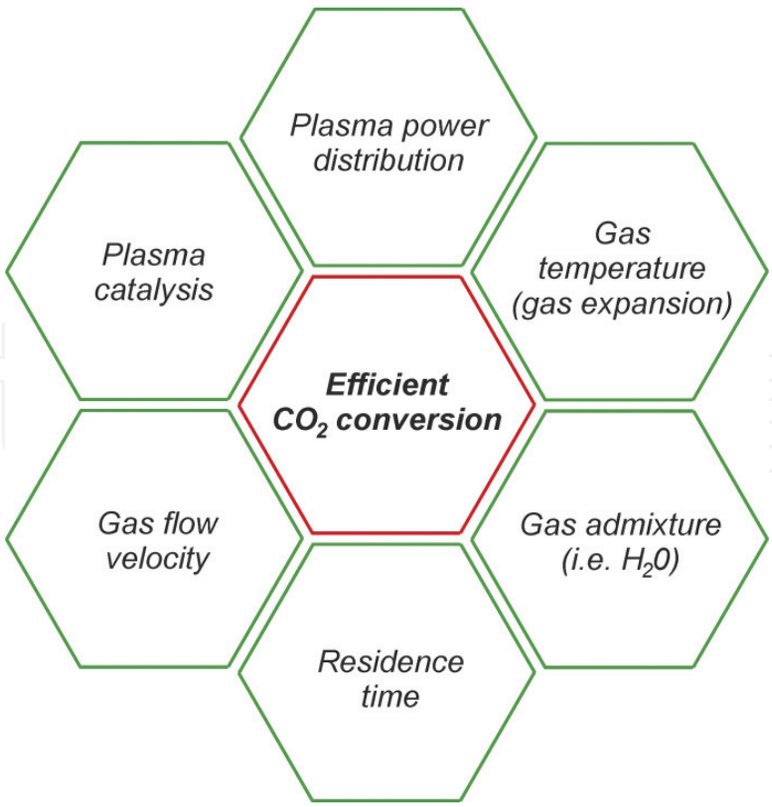

Figure 11. Summary of the critical factors influencing CO_2 conversion in microwave flowing gas discharges.

transfer rates, and thus the vibrational distributions of the molecules of interest. This work is supposed to be assisted by plasma modeling targeted at clarification of the numerous important kinetic processes.

Finally, the plasma catalysis activities are supposed to be especially beneficial since an essential gain in the CO_2 conversion efficiency can be achieved in this case. As shown recently [14, 28], the regenerative properties of the Ni-based catalysts are the microwave plasma combined with their long lifetime [51] enable roughly a twofold increase in the overall CO_2 conversion and energy efficiencies. The questions related to the utilization of plasma catalysis for improvements of the CO_2 conversion efficiency are discussed in the following chapter.

6. Conclusions

Several physical aspects related to the power modulation during the plasma-assisted conversion of CO_2 in the low-to-moderate pressure flowing gas microwave discharges are discussed. The beneficial effects of controlling the plasma pulse frequency (in the vicinity of 1 kHz or lower in our case) for increasing the CO_2 conversion efficiency are clearly demonstrated.

In particular, it was shown that by tuning the plasma pulse repetition frequency, the CO_2 conversion and energy efficiencies can be improved several times. In the 2.45-GHz plasma system, a fourfold overall improvement has been registered. Based on the estimations of the characteristic time corresponding to the relevant energy transfer processes for the studied pulse frequency range (0.5–30 kHz), it was concluded that the electron-vibrational as well as vibrational-translational energy transfer mechanisms are mainly responsible for the optimization of CO_2 conversion in a flowing gas microwave discharge. A resonant-like relation between the characteristic time of the mentioned processes and the plasma pulse-on time may lead to either high or low CO_2 decomposition efficiency, depending on the plasma pulse frequency. The maximum efficiency found so far corresponds to the frequencies of about 0.5–0.8 kHz depending on the studied plasma source.

At the same time, the gas temperature in the discharge active zone (i.e., near the excitation point) is supposed to be strongly influenced by the V-T and e-T energy transfer, as well as by the O atoms recombination at low repetition frequencies. Under these conditions at the beginning of the postdischarge, the gas temperature is somewhat reduced, as compared to the high frequency case. At high pulse frequency, the gas temperature in the active zone is getting lower by few hundreds degree K, presumably mainly due to the reduced O recombination (which is an exothermic process), whereas at the end of the discharge tube, it elevates following the O atom density, which is higher in this case. Numerous processes involving O atom kinetics should be studied by modeling, however, before clarifying this question fully.

In addition to the modulated microwave power delivery to the discharge, studied in this work, the other ways of optimization of the MW plasma-based CO_2 conversion are suggested. Among them are the optimizations related to the gas residence time, plasma pulse duty ratio, gas admixture, gas expansion in the discharge tube, and plasma catalysis. The results described in this chapter, combined with the suggested ways for the CO_2 conversion

improvements are supposed to be useful for the industry-oriented applications dealing with a local plasma-assisted CO_2 conversion.

Acknowledgements

This study is supported by Belgian Government through the "Pôle d'Attraction Interuniversitaire" (PAI, P7/34, "Plasma-Surface Interaction," PSI). In addition, the partial support of the following projects should be acknowledged: the "REFORGAS GreenWin" project, grant No. 7267, (for N.B., G.C., T.G.), as well as the Portuguese FCT, under the projects UID/FIS/50010/2013 and PTDC/FIS-PLA/1420/2014 (for T.S.).

Author details

Nikolay Britun[1]*, Guoxing Chen[1,2], Tiago Silva[3], Thomas Godfroid[4], Marie-Paule Delplancke-Ogletree[2] and Rony Snyders[1,4]

*Address all correspondence to: nikolay.britun@umons.ac.be

1 Chimie des Interactions Plasma Surface, University of Mons, Belgium

2 4MAT, Université Libre de Bruxelles, Belgium

3 Instituto de Plasmas e Fusão Nuclear, University of Lisbon, Portugal

4 Materia Nova Research Center, Belgium

References

[1] R. M. Cuéllar-Franca and A. Azapagic, J. CO_2 Utilization **9**, 82 (2015).

[2] A. P. H. Goede, EPJ Web Conf. **98**, 7002 (2015).

[3] N. Britun, T. Minea, S. Konstantinidis, and R. Snyders, J. Phys. D Appl. Phys. **47**, 224001 (2014).

[4] A. Bogaerts, C. De Bie, R. Snoeckx, and T. Kozák, Plasma Process. Polym. DOI: 10.1002/ppap.201600070 (2016).

[5] A. A. Fridman and L. A. Kennedy, *Plasma Physics and Engineering* (Taylor and Francis, New York, 2011).

[6] A. A. Fridman, *Plasma Chemistry* (Cambridge University Press, New York, 2005).

[7] V. D. Rusanov, A. A. Fridman, and G. V Sholin, Sov. Phys. Uspekhi **24**, 447 (1981).

[8] V. N. Ochkin, *Spectroscopy of Low Temperature Plasma* (Wiley-VCH, Weinheim, 2009).

[9] Y. A. Lebedev, J. Phys. Conf. Ser. **257**, 12016 (2010).

[10] V. A. Legasov, *Nuclear – Hydrogen Energy and Technology. Vol. 1.* (Atom-Izdat, Moscow, 1978).

[11] R. I. Asisov, A. K. Vakar, V. K. Jivotov, et al., Proc. USSR Acad. Sci. **271**, 94 (1983).

[12] A. Fridman, S. Nester, L. A. Kennedy, A. Saveliev, and O. Mutaf-Yardimci, Prog. Energy Combust. Sci. **25**, 211 (1999).

[13] T. Godfroid, J. P. Dauchot, and M. Hecq, Surf. Coatings Technol. **200**, 649 (2005).

[14] G. Chen, N. Britun, T. Godfroid, V. Georgieva, R. Snyders, and M.-P. Delplancke, J. Phys. D Appl. Phys. **50**, 084001 (2017).

[15] T. Silva, N. Britun, T. Godfroid, and R. Snyders, Plasma Sources Sci. Technol. **23**, 025009 (2014).

[16] R. Aerts, W. Somers, and A. Bogaerts, Chem Sus Chem **8**, 702 (2015).

[17] S. Paulussen, B. Verheyde, X. Tu, C. De Bie, T. Martens, D. Petrovic, A. Bogaerts, and B. Sels, Plasma Sources Sci. Technol. **19**, 034015 (2010).

[18] A. Ozkan, T. Dufour, T. Silva, N. Britun, R. Snyders, F. Reniers, and A. Bogaerts, Plasma Sources Sci. Technol. **25**, 055005 (2016).

[19] A. Ozkan, T. Dufour, T. Silva, N. Britun, R. Snyders, A. Bogaerts, and F. Reniers, Plasma Sources Sci. Technol. **25**, 025013 (2016).

[20] D. Mei, Y.-L. He, S. Liu, J. Yan, and X. Tu, Plasma Process. Polym. **13**, 544 (2016).

[21] X. Duan, Y. Li, W. Ge, and B. Wang, Greenh. Gases Sci. Technol. **5**, 131 (2015).

[22] T. Nunnally, K. Gutsol, A. Rabinovich, A. Fridman, A. Gutsol, and A. Kemoun, J. Phys. D. Appl. Phys. **44**, 274009 (2011).

[23] A. Indarto, D. R. Yang, J.-W. Choi, H. Lee, and H. K. Song, J. Hazard. Mater. **146**, 309 (2007).

[24] S. R. Sun, H. X. Wang, D. H. Mei, X. Tu, and A. Bogaerts, J. CO_2 Utilization **17**, 220 (2017).

[25] L. F. Spencer and A. D. Gallimore, Plasma Chem. Plasma Process. **31**, 79 (2011).

[26] L. F. Spencer and A. D. Gallimore, Plasma Sources Sci. Technol. **22**, 015019 (2013).

[27] S. Mahammadunnisa, E. L. Reddy, D. Ray, C. Subrahmanyam, and J. C. Whitehead, Int. J. Greenh. Gas Control **16**, 361 (2013).

[28] G. Chen, T. Godfroid, N. Britun, V. Georgieva, M.-P. Delplancke, and R. Snyders, Appl. Catal. B. Environ. *Submitted* (2017).

[29] T. Kozák and A. Bogaerts, Plasma Sources Sci. Technol. **23**, 045004 (2014).

[30] J. A. Blauer and G. R. Nickerson, Rep. Ultrasystems Inc. (1973).

[31] K. Kutasi, V. Guerra, and P. Sá, J. Phys. D. Appl. Phys. **43**, 175201 (2010).

[32] J. G. Parker, Phys. Fluids **2**, 449 (1959).

[33] T. Silva, N. Britun, T. Godfroid, J. van der Mullen, and R. Snyders, J. Appl. Phys. **119**, 173302 (2016).

[34] SIGLO Database, www.lxcat.net, Retrieved Nov 24, 2016.

[35] R. C. Millikan and D. R. White, J. Chem. Phys. **39**, 3209 (1963).

[36] B. Chapman, *Glow Discharge Processes* (John Wiley & Sons, Ltd, New York, 1980).

[37] Phelps Database, www.lxcat.net, Retrieved Nov 24, 2016.

[38] M. Moisan and Z. Zakrzewski, J. Phys. D. Appl. Phys. **24**, 1025 (1991).

[39] G. Chen, V. Georgieva, T. Godfroid, R. Snyders, and M. P. Delplancke-Ogletree, Appl. Catal. B Environ. **190**, 115 (2016).

[40] T. Silva, N. Britun, T. Godfroid, and R. Snyders, Opt. Lett. **39**, 6146 (2014).

[41] G. F. Kirkbright and M. Sargent, *Atomic Absorption and Fluorescence Spectroscopy* (Academic Press, London, 1974).

[42] K. Niemi, V. S. Der Gathen, and H. F. Döbele, J. Phys. D. Appl. Phys. **34**, 2330 (2001).

[43] J. Rosell, J. Sjöholm, M. Richter, and M. Aldén, Appl. Spectrosc. **67**, 314 (2013).

[44] R. W. B. Pearse and A. G. Gaydon, *The Identification of Molecular Spectra*, 4th ed. (Chapman and Hall, London, 1976).

[45] C. Rond, A. Bultel, P. Boubert, and B. G. Chéron, Chem. Phys. **354**, 16 (2008).

[46] A. V Eremin and V. S. Ziborov, J. Appl. Mech. Tech. Phys. **34**, 752 (1993).

[47] N. Britun, M. Palmucci, S. Konstantinidis, M. Gaillard, and R. Snyders, J. Appl. Phys. **114**, 013301 (2013).

[48] G. Chen, T. Silva, V. Georgieva, T. Godfroid, N. Britun, R. Snyders, and M. P. Delplancke-Ogletree, Int. J. Hydrogen Energy **40**, 3789 (2015).

[49] T. Silva, N. Britun, T. Godfroid, and R. Snyders, Plasma Process. Polym. DOI: 10.1002/ppap.201600103 (2016).

[50] D. Marinov, D. Lopatik, O. Guaitella, M. Hübner, Y. Ionikh, J. Röpcke, and A. Rousseau, J. Phys. D. Appl. Phys. **45**, 175201 (2012).

[51] M. Zhang, D.-G. Cheng, and Y.-P. Zhang, Prepr. Pap.-Am. Chem. Soc., Div. Fuel Chem. **49**, 188 (2004).

IntechOpen